Electronic Supporting Information

Coordination Chemistry of Hepta-tert-*butylnonaphosphane*

Volker Eilrich, Toni Grell, Peter Lönnecke and Evamarie Hey-Hawkins

Content

1. DFT Calculations

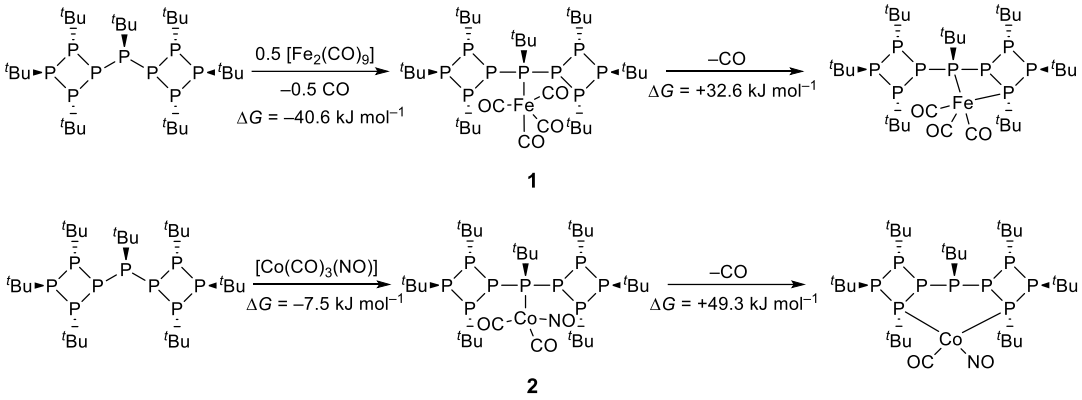

Scheme S1 Calculated energies for the formation of the hypothetical bidentate iron and cobalt complexes formed from complexes **1** and **2**. The energy of the most stable configuration of the respective hypothetical complexes with bidentate bonding mode was used (see below, Scheme S4).

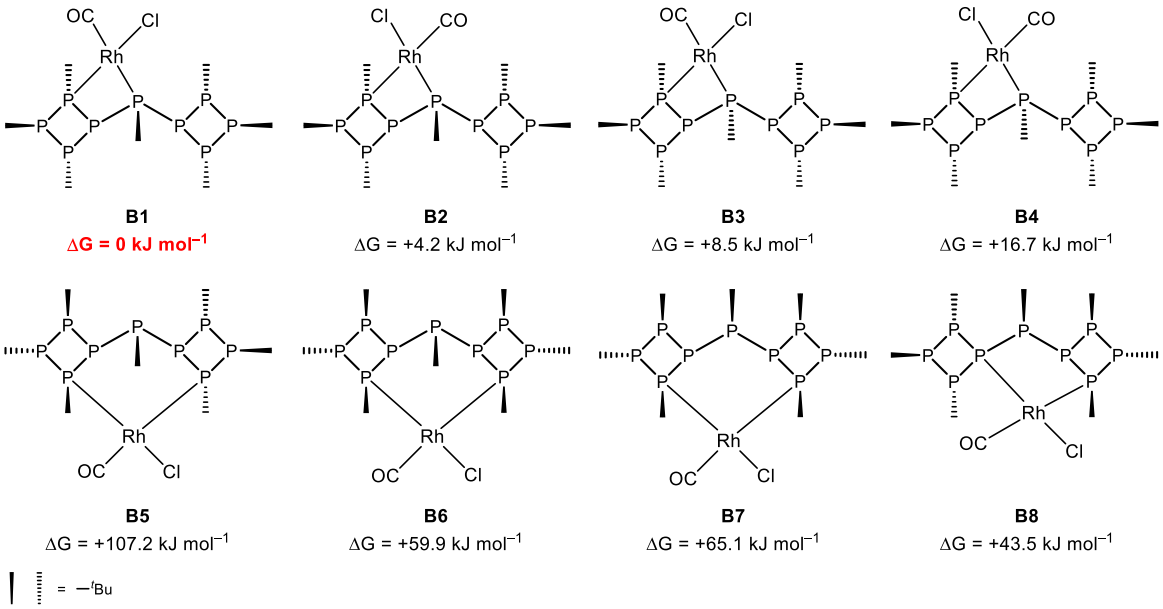

Scheme S2 Structural formulas and relative energies of all possible configurational isomers of the bidentate rhodium complex **4**. Configurations according to the different bidentate bonding modes are labelled **B1–B8**. Minimum energies are labelled in red.

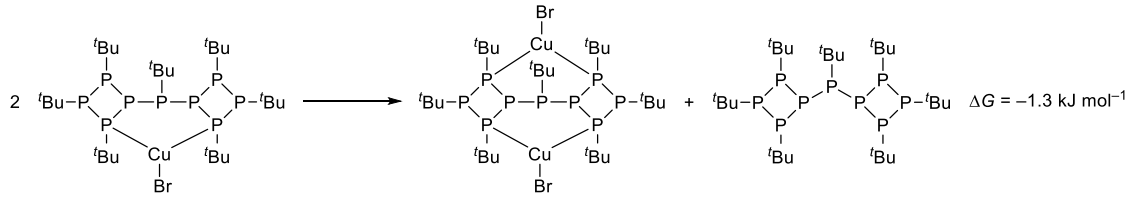

Scheme S3 Two molecules of the mononuclear copper(I) complex react to give one molecule of **3** and one molecule of the ligand **L**. To find the most stable configuration of the mononuclear bidentate complex, the different configurations analogous to Scheme S2 were calculated. The most stable configuration corresponds to **B7**, which was used to calculate this reaction energy.

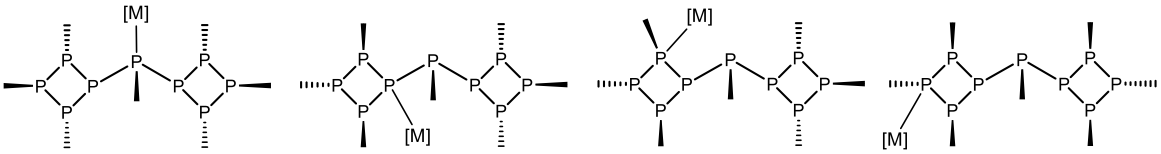

M1

[M] = $Fe(CO)_4$:
ΔG = 0 kJ mol^{-1}
[M] = $Co(NO)(CO)_2$:
ΔG = 0 kJ mol^{-1}

M2

[M] = $Fe(CO)_4$:
ΔG = +53.9 kJ mol^{-1}
[M] = $Co(NO)(CO)_2$:
ΔG = +69.3 kJ mol^{-1}

M3

[M] = $Fe(CO)_4$:
ΔG = +27.6 kJ mol^{-1}
[M] = $Co(NO)(CO)_2$:
ΔG = +36.9 kJ mol^{-1}

M4

[M] = $Fe(CO)_4$:
ΔG = +26.9 kJ mol^{-1}
[M] = $Co(NO)(CO)_2$:
ΔG = +53.3 kJ mol^{-1}

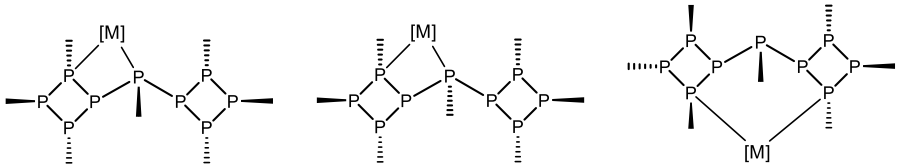

B1 = B2

[M] = $Fe(CO)_3$:
ΔG = 0 kJ mol^{-1}
[M] = Co(NO)(CO):
ΔG = +7.4 kJ mol^{-1}

B3 = B4

[M] = $Fe(CO)_3$:
ΔG = + 9.9 kJ mol^{-1}
[M] = Co(NO)(CO):
ΔG = +13.5 kJ mol^{-1}

B5

[M] = $Fe(CO)_3$:
ΔG = + 60.3 kJ mol^{-1}
[M] = Co(NO)(CO):
ΔG = +43.1 kJ mol^{-1}

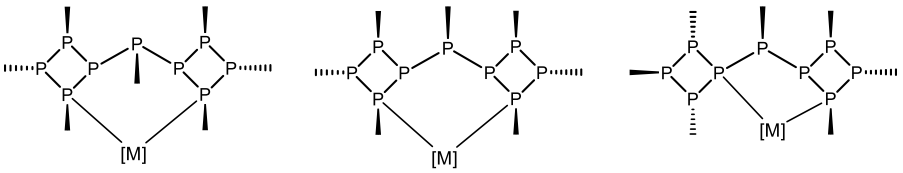

B6

[M] = $Fe(CO)_3$:
ΔG = + 66.6 kJ mol^{-1}
[M] = Co(NO)(CO):
ΔG = +5.5 kJ mol^{-1}

B7

[M] = $Fe(CO)_3$:
ΔG = + 45.0 kJ mol^{-1}
[M] = Co(NO)(CO):
ΔG = 0 kJ mol^{-1}

B8

[M] = $Fe(CO)_3$:
ΔG = + 51.2 kJ mol^{-1}
[M] = Co(NO)(CO):
ΔG = +13.7 kJ mol^{-1}

= $-{}^t$Bu

Scheme S4 Structural formulas and relative energies of all possible constitutional isomers of the monodentante iron and cobalt complexes **1** and **2** (top) as well as the configurational isomers of their hypothetical bidentate complexes (bottom). Minimum energies are labelled in red. Constitutions according to monodentate bonding modes are labelled **M1–M4**. Configurations of the bidentate bonding modes are labelled **B1–B8**, in analogy to the ones calculated for the rhodium complex **4**. It should be noted, that due to the different coordination environment in case of iron and cobalt, the configurations **B1** and **B2** as well as **B3** and **B4** are identical (different input structures yielded the same result).

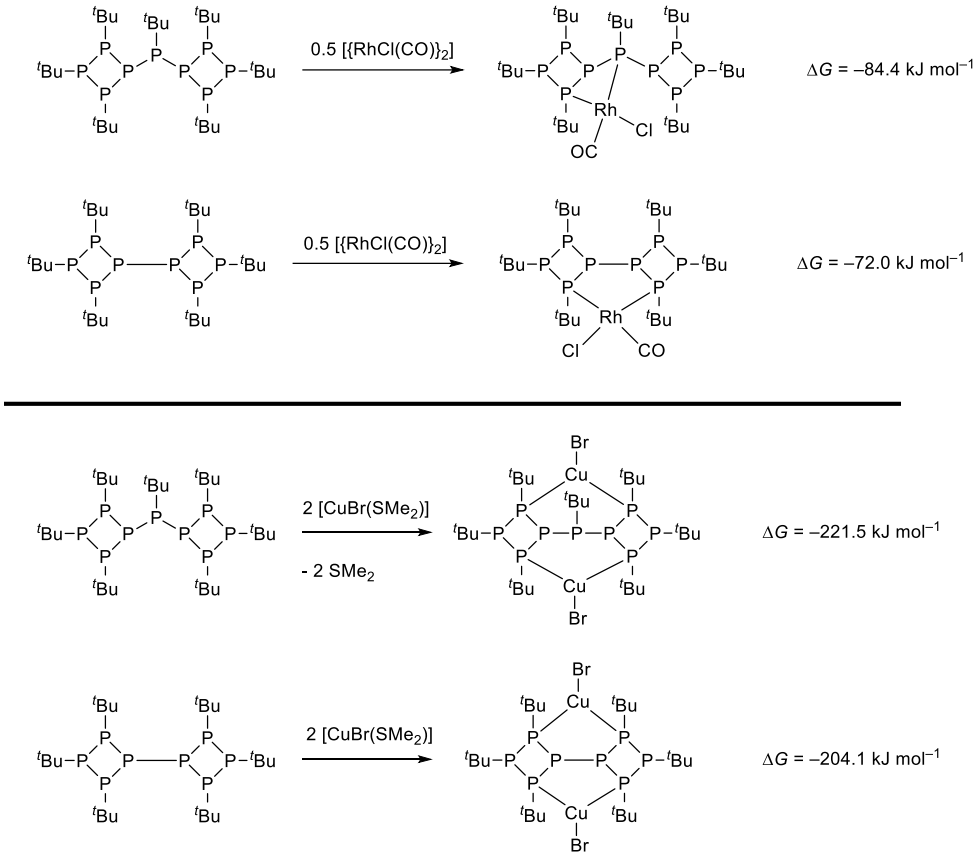

Scheme S5 Calculated energies for the formation of complex **3** and **4** and their analogues with {*cyclo*-($P_4^{t}Bu_3$)}$_2$. For the latter two, the energies were already determined before[1] but were recalculated with the optimised benchmarked combination (Table S1) to allow an accurate comparison. The most stable configuration **B1** was used for complex **3**.

Table S1 Results from the benchmarking to find the best functional and basis set combination based on the CO stretching vibration of complex **4**.

Method	CO stretching vibration (cm^{-1})
Experiment	1996.5
BP86/def2-SVP	1967.6
B3LYP/def2-TZVP	2028.7
M06L/def2-TZVP	1977.4
TPPS/def2-TZVP	1955.5
TPPSh/def2-TZVP	**2004.0**
PBE0/def2-TZVP	2065.8

[1] T. Grell and E. Hey-Hawkins, *Inorg. Chem.*, 2020, **59**, 7487.

2. TG-DTA Analysis

2.1. [Fe(CO)$_4$({*cyclo*-(P$_4$^{t}Bu$_3$)}$_2$P^{t}Bu-κ*P*^{9})] (1)

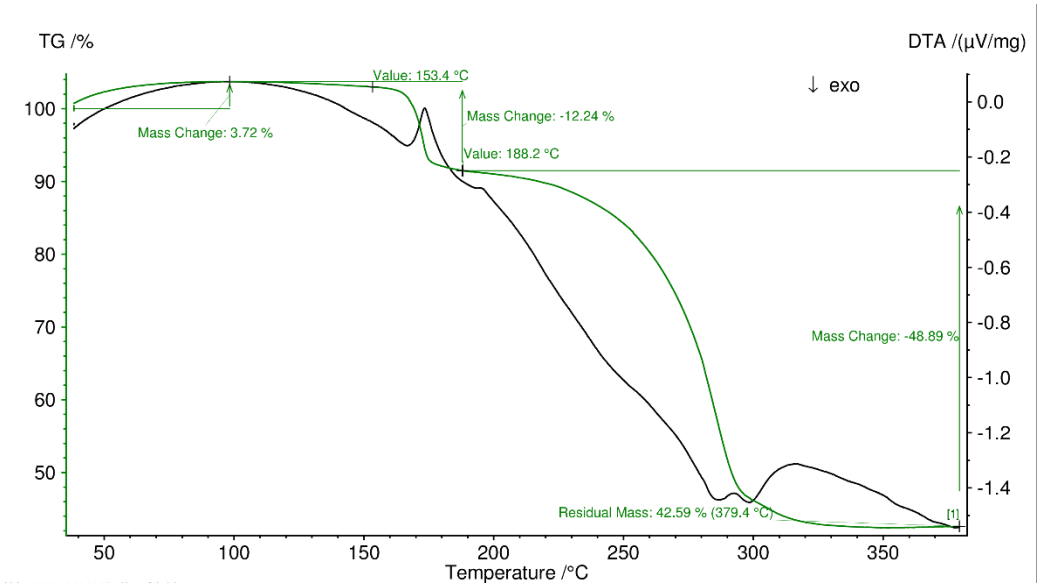

Fig. S1 TG-DTA of **1**.

2.2. [Co(CO)$_2$(NO)({*cyclo*-(P$_4$^{t}Bu$_3$)}$_2$P^{t}Bu-κ*P*^{9})] (2)

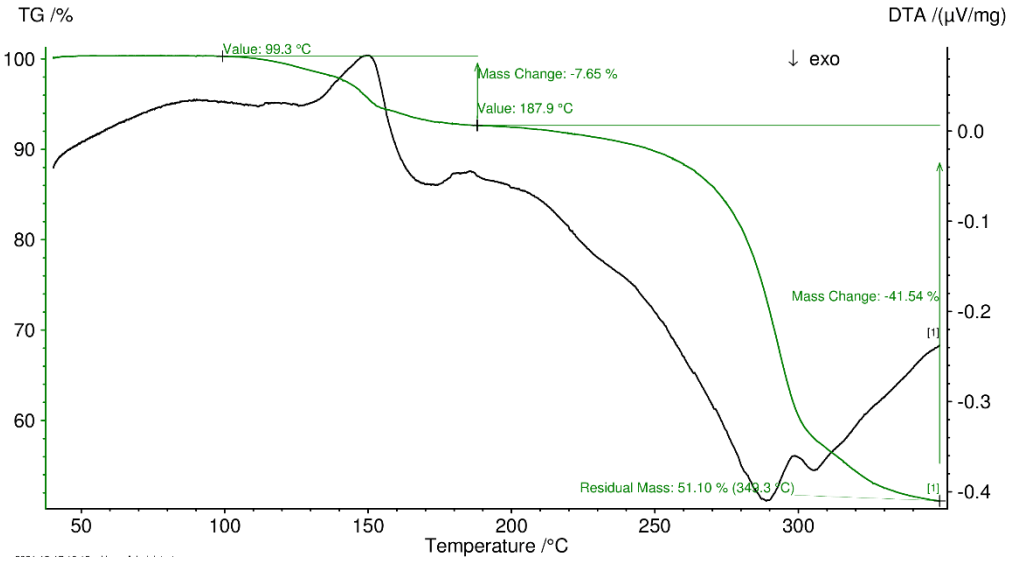

Fig. S2 TG-DTA of **2**.

2.3. [(CuBr)$_2$({*cyclo*-(P$_4$^{t}Bu$_3$)}$_2$P^{t}Bu-κ^2*P*^{2},*P*^{7},κ^2*P*^{3},*P*^{6})}] (3)

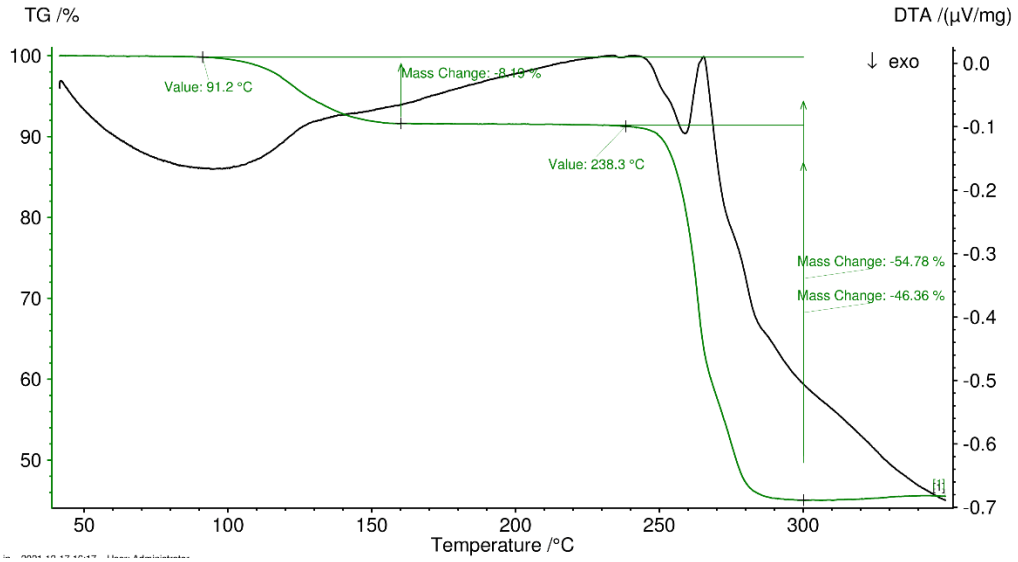

Fig. S3 TG-DTA of **3**.

2.4. [RhCl(CO)({*cyclo*-(P$_4$^{t}Bu$_3$)}$_2$P^{t}Bu-κ^2*P*^{6},*P*^{9})] (4)

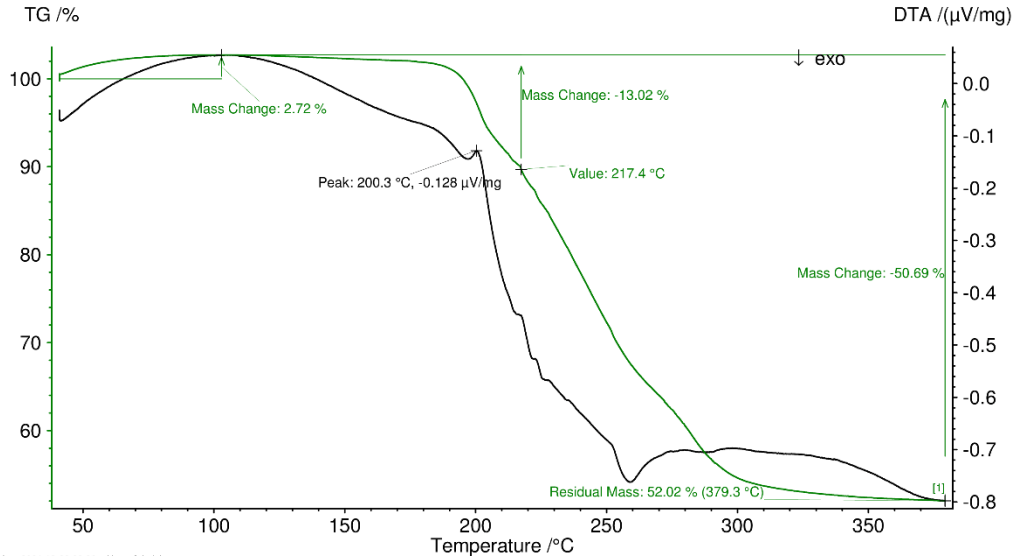

Fig. S4 TG-DTA of **4**.

3. Single Crystal X-Ray Diffraction

Table S2 Summary of Crystallographic Data Obtained from Single-Crystal X-Ray Diffraction.

Compound	**1**	**2**	**3**·C_4H_8O	**4**	**5**
Empirical formula	$C_{32}H_{63}FeO_4P_9$	$C_{30}H_{63}CoNO_3P_9$	$C_{32}H_{71}Br_2Cu_2OP_9$	$C_{29}H_{63}ClOP_9Rh$	$C_{28}H_{63}Cl_2P_9Pd$
Formula weight	846.40	823.47	1037.51	844.48	855.81
Temperature [K]	130(2)	130(2)	130(2)	130(2)	130(2)
Wavelength [pm]	71.073	71.073	71.073	71.073	71.073
Crystal system	Monoclinic	Triclinic	Monoclinic	Monoclinic	Monoclinic
Space group	*I*2/*a*	$P\bar{1}$	$P2_1/c$	$P2_1/c$	$P2_1/c$
Unit cell					
a [pm]	1846.95(3)	1123.70(3)	1154.77(1)	2376.32(3)	2398.98(8)
b [pm]	1030.08(1)	1992.94(5)	1955.29(3)	922.05(1)	904.93(3)
c [pm]	2385.12(4)	2199.07(5)	2087.09(3)	1952.00(3)	1954.63(8)
α [deg]	90	110.379(2)	90	90	90
β [deg]	103.481(2)	96.610(2)	99.633(1)	99.045(1)	99.562(3)
γ [deg]	90	105.435(2)	90	90	90
Volume [nm^3]	4.4127(1)	4.3307(2)	4.6460(1)	4.2279(1)	4.1844(3)
Z	4	4	4	4	4
ρ (calc) [Mg/m^3]	1.274	1.263	1.483	1.327	1.358
μ mm^{-1}	0.700	0.758	2.970	0.829	0.934
F(000)	1792	1744	2136	1768	1784
Crystal size [mm^3]	0.40 x 0.30 x 0.20	0.20 x 0.20 x 0.07	0.40 x 0.40 x 0.30	0.30 x 0.20 x 0.03	0.15 x 0.08 x 0.02
Θ min / *Θ* max [deg]	1.756 / 34.683	1.814 / 29.047	1.789 / 34.754	2.113 / 32.374	1.722 / 28.527
Index ranges	$-29 \le h \le 27$	$-14 \le h \le 14$	$-18 \le h \le 17$	$-35 \le h \le 35$	$-28 \le h \le 31$
	$-16 \le k \le 16$	$-26 \le k \le 27$	$-31 \le k \le 31$	$-13 \le k \le 13$	$-11 \le k \le 12$
	$-37 \le l \le 37$	$-29 \le l \le 28$	$-33 \le l \le 32$	$-28 \le l \le 28$	$-25 \le l \le 25$
Reflections collected	42537	57339	112352	103742	31603
Independent reflections [R(int)]	9070 [0.0312]	20272 [0.0562]	19149 [0. 0440]	14390 [0.0629]	9657 [0.0987]
Completeness [%] (*Θ*) [deg]	100 (33.140)	100 (26.375)	100 (33.140)	100 (30.510)	100 (26.375)
T_{Max} / T_{Min}	1.00000 / 0.84931	1.00000 / 0.92285	1.00000 / 0.67185	1.00000 / 0.92353	1.00000 / 0.68164
Restraints / parameters	10 / 256	0 / 835	51 / 469	0 / 391	0 / 382
Goodness-of-fit on F^2	1.231	1.019	1.057	1.050	0.995
R_1, wR_2 [I > 2σ(*I*)]	0.0666, 0.1484	0.0534, 0.1213	0.0365, 0.0791	0.0411, 0.0777	0.0511, 0.0867
R indices (all data)	0.0769, 0.1523	0.0994, 0.1442	0.0676, 0.0942	0.0577, 0.0831	0.1064, 0.1070
Residual electron density [$e \cdot Å^{-3}$]	0.619 / –0.536	1.115 / –0.862	0.985 / –0.740	1.141 / –0.520	0.812 / –1.188
CCDC number	2144600	2144601	2144602	2144603	2144604

4. NMR Spectra

4.1. [Fe(CO)$_4$({*cyclo*-(P$_4$^{t}Bu$_3$)}$_2$P^{t}Bu-κ*P*^{9})] (1)

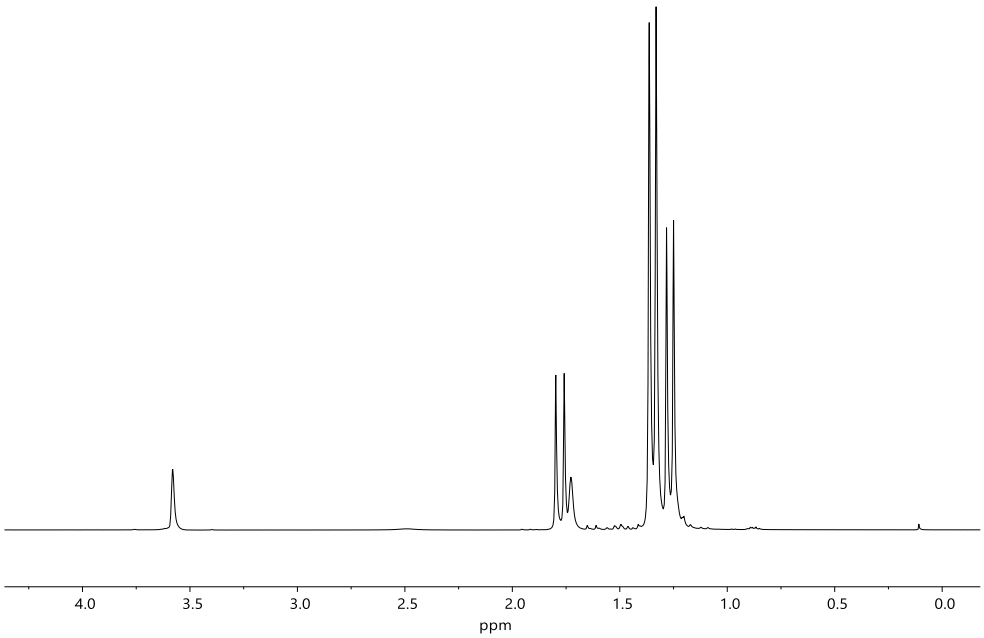

Fig. S5 ^{1}H NMR spectrum of **1** in THF-*d*^{8} (400 MHz).

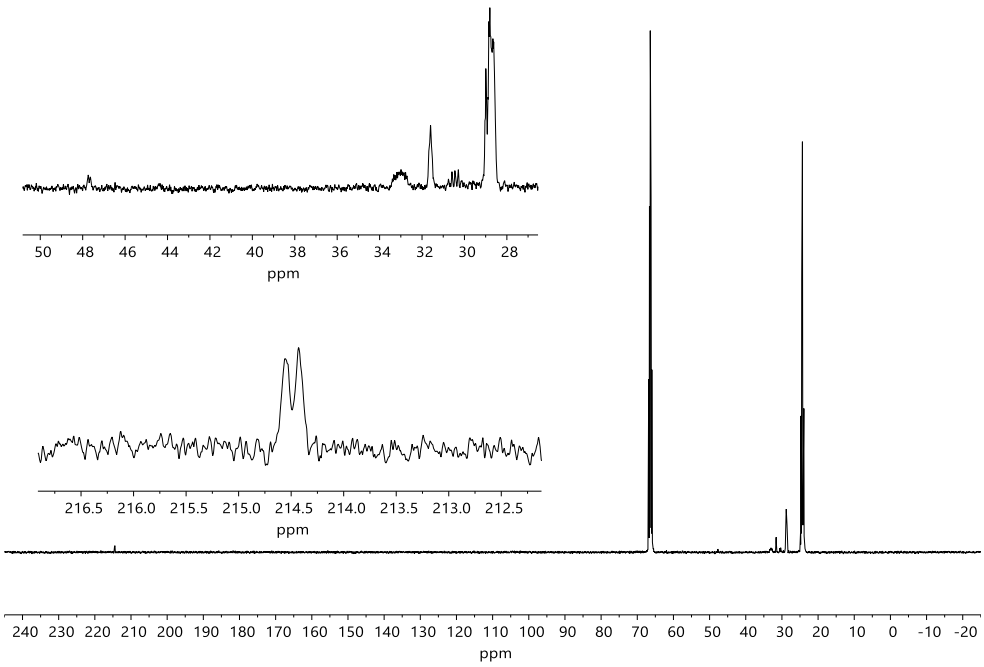

Fig. S6 ^{13}C{^{1}H} NMR spectrum of **1** in THF-*d*^{8} (101 MHz).

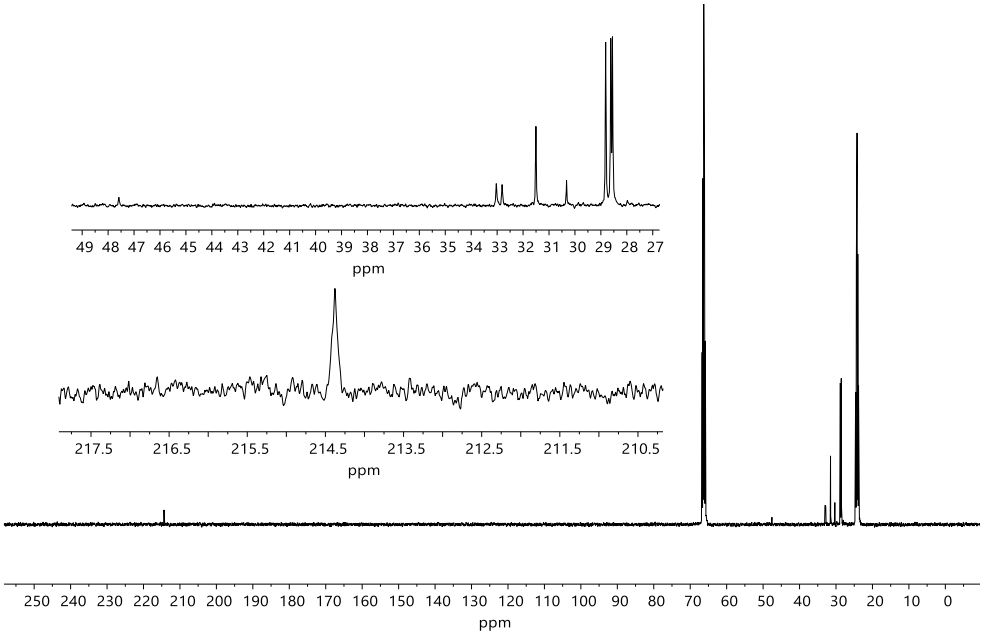

Fig. S7 $^{13}C\{^{1}H,^{31}P\}$ NMR spectrum of **1** in THF-d^8 (101 MHz) at 28 °C.

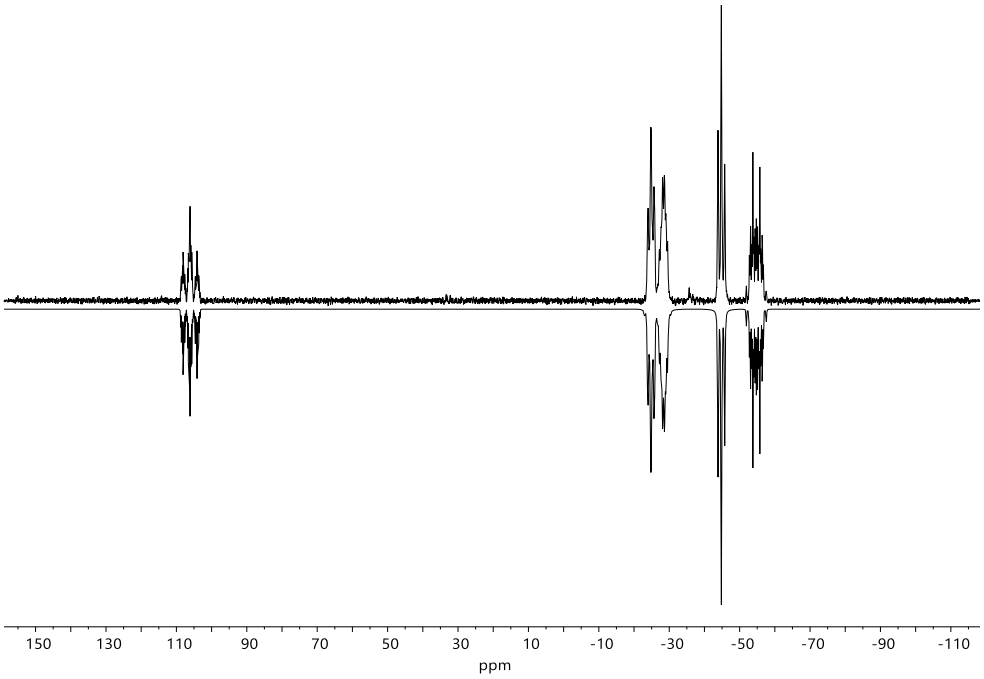

Fig. S8 Experimental (top) and simulated (bottom) $^{31}P\{^{1}H\}$ NMR spectrum of **1** in THF-d^8 (162 MHz).

4.2. $[Co(CO)_2(NO)(\{cyclo\text{-}(P_4{}^tBu_3)\}_2P^tBu\text{-}\kappa P^9)]$ (2)

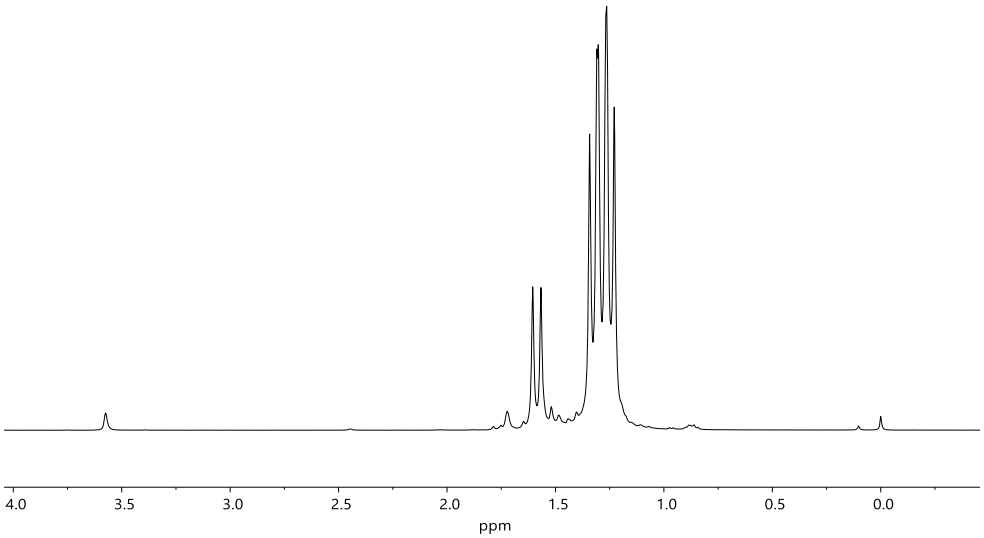

Fig. S9 ^1H NMR spectrum of **2** in THF-d^8 (400 MHz).

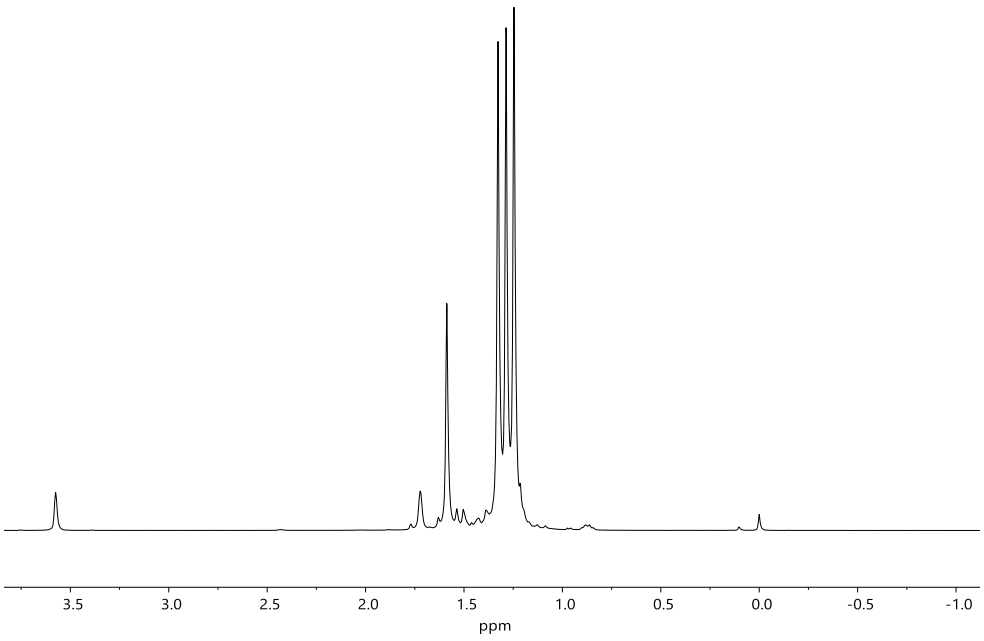

Fig. S10 $^1H\{^{31}P\}$ NMR spectrum of **2** in THF-d^8 (400 MHz).

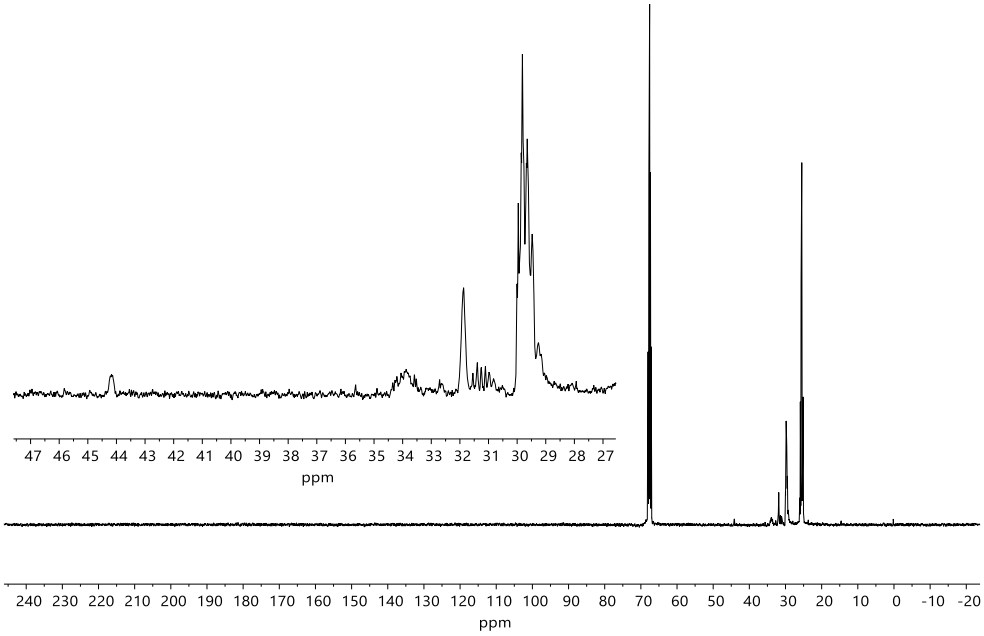

Fig. S11 $^{13}C\{^{1}H\}$ NMR spectrum of **2** in THF-d^8 (101 MHz).

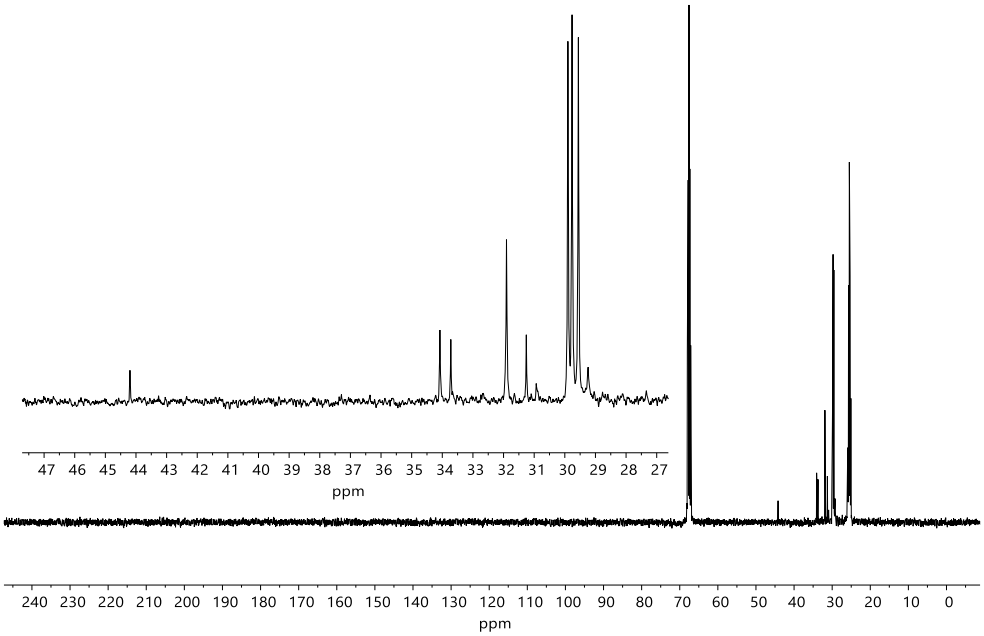

Fig. S12 $^{13}C\{^{1}H,^{31}P\}$ NMR spectrum of **2** in THF-d^8 (101 MHz) at 28 °C.

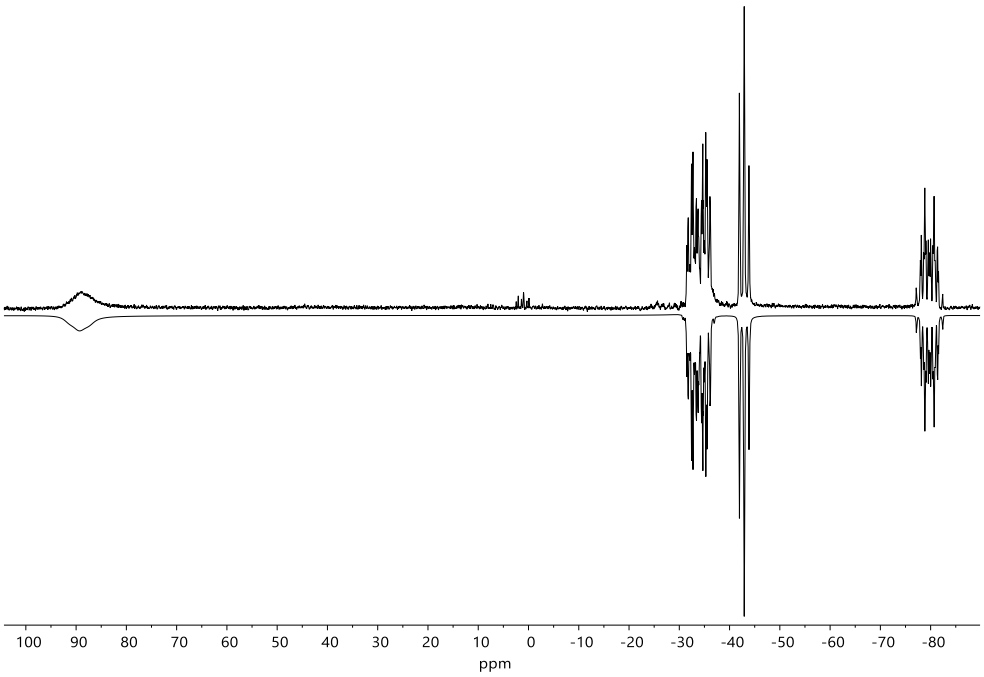

Fig. S13 Experimental (top) and simulated (bottom) $^{31}P\{^{1}H\}$ NMR spectrum of **2** in THF-d^8 (162 MHz).

4.3. [(CuBr)$_2$({*cyclo*-(P$_4$^{t}Bu$_3$)}$_2$P^{t}Bu-κ^2*P*^{2},*P*^{7},κ^2*P*^{3},*P*^{6})}] (3)

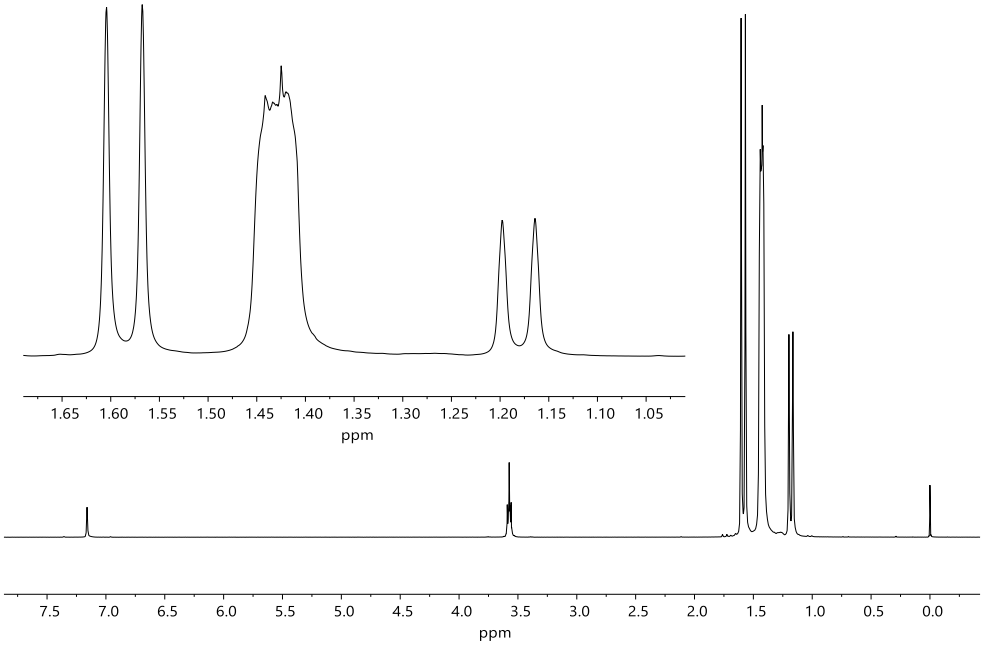

Fig. S14 ^{1}H NMR spectrum of **3** in benzene-d^6 (400 MHz).

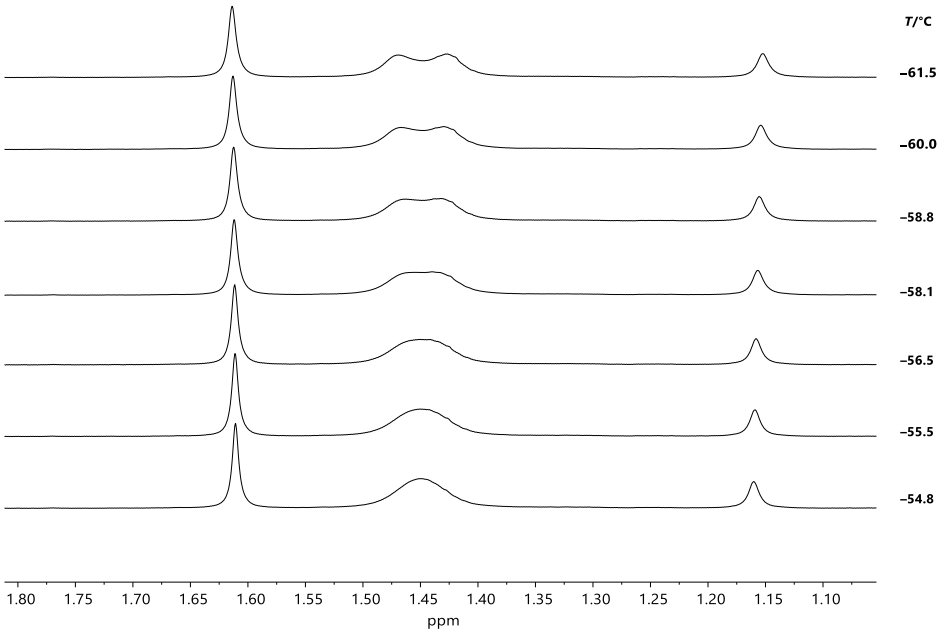

Fig. S15 Excerpt of the $^{1}H\{^{31}P\}$ VT NMR spectra of **3** in toluene-d^8, conducted with methanol (capillary) as internal standard for the temperature calibration. $\Delta\nu_{AB}$ of the resonances at 1.45 ppm is found to be 20.5 Hz at –66.8 °C.

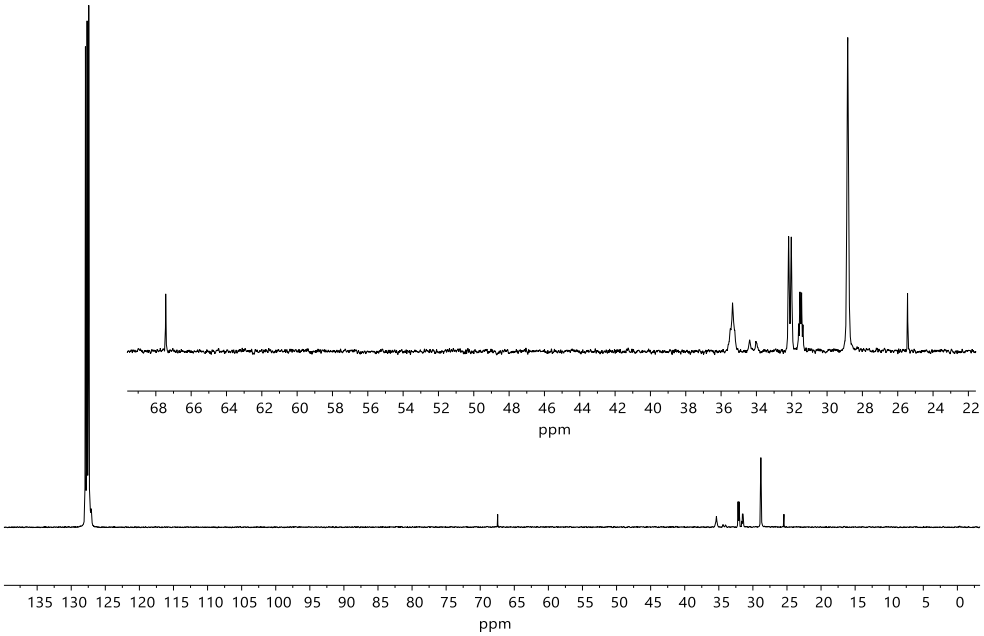

Fig. S16 $^{13}C\{^{1}H\}$ NMR spectrum of **3** in benzene-d^6 (101 MHz).

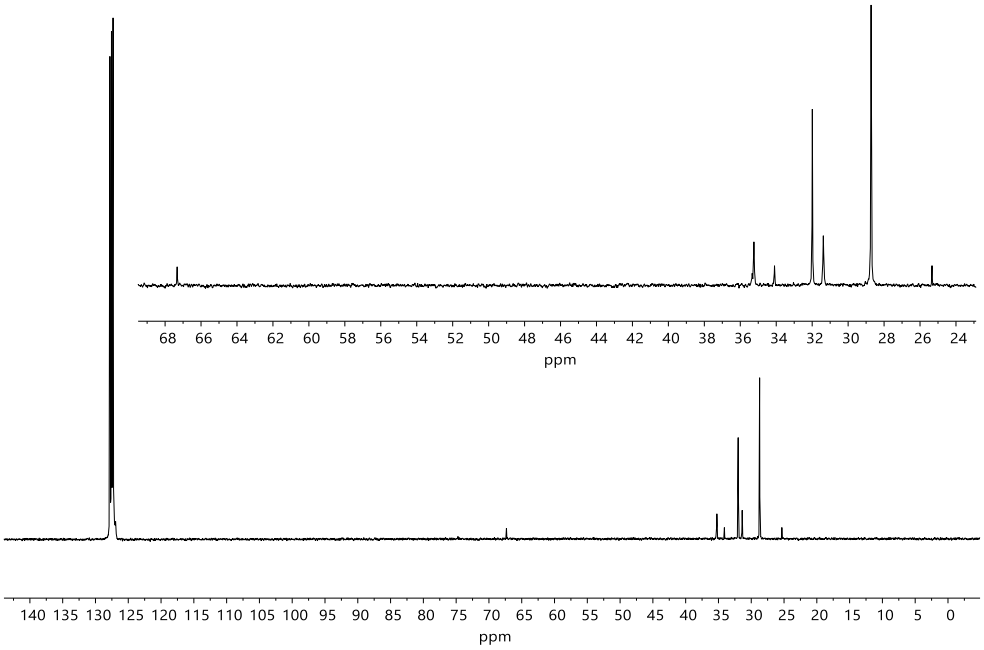

Fig. S17 $^{13}C\{^{1}H,^{31}P\}$ NMR spectrum of **3** in benzene-d^6 (101 MHz) at 28 °C.

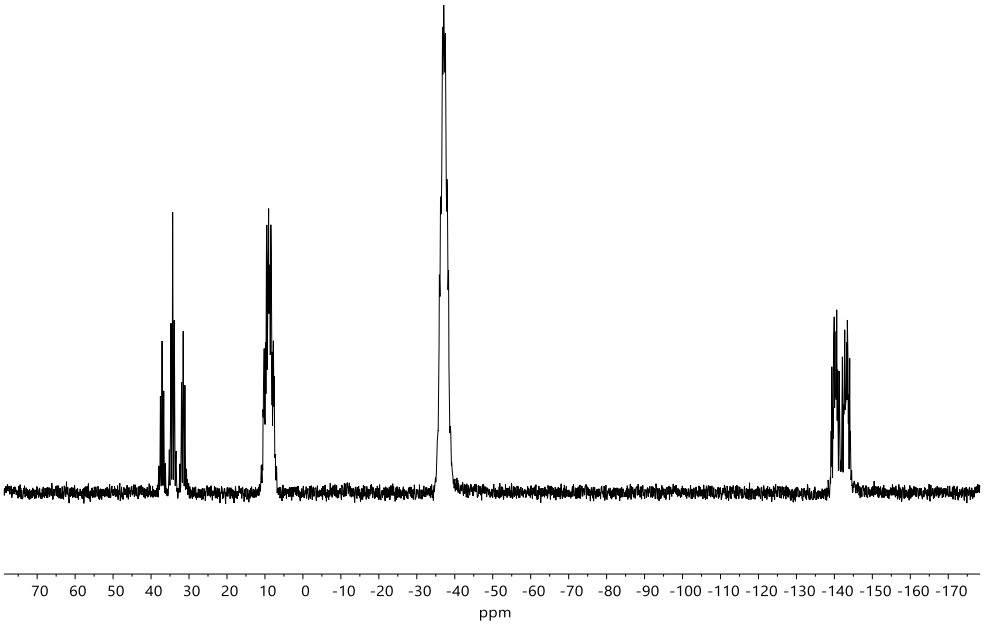

Fig. S18 $^{31}P\{^{1}H\}$ NMR spectrum of **3** in benzene-d^6 (162 MHz).

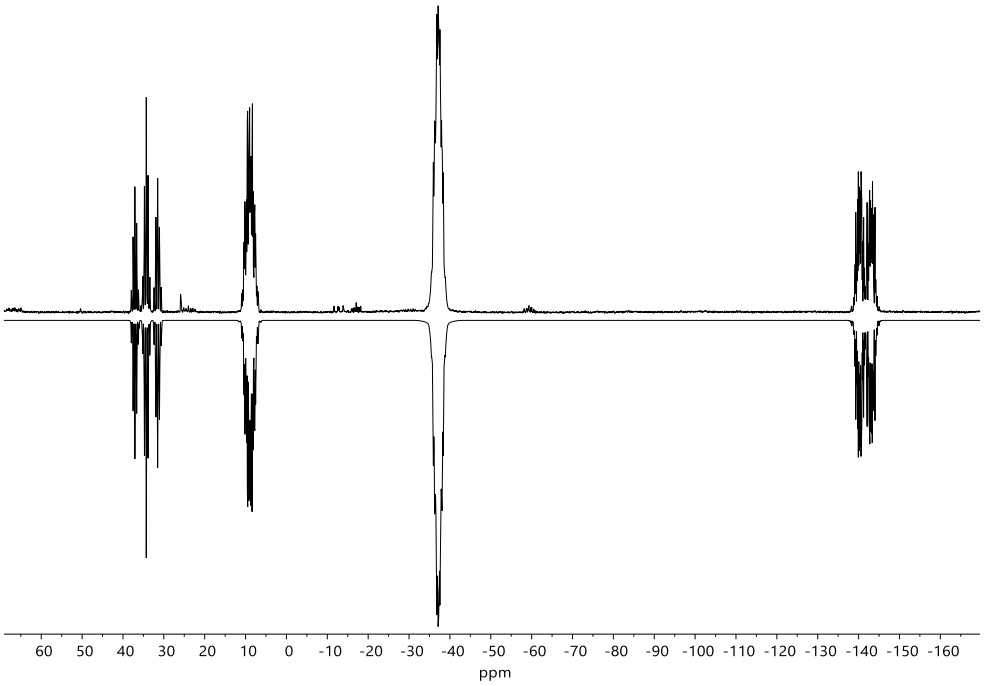

Fig. S19 Experimental (top) and simulated (bottom) $^{31}P\{^{1}H\}$ NMR spectrum of **3** in benzene-d^6 (162 MHz).

4.4. [RhCl(CO)({*cyclo*-($P_4{}^tBu_3$)}$_2$$P^tBu$-κ^2*P*^{6},*P*^{9})] (4)

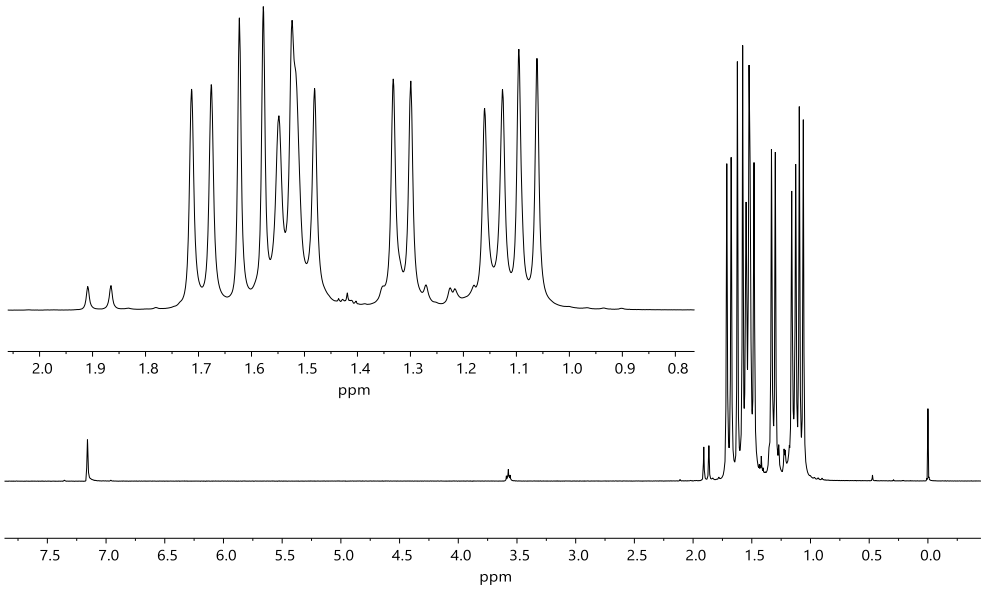

Fig. S20 ^{1}H NMR spectrum of **4** in benzene-d^6 (400 MHz).

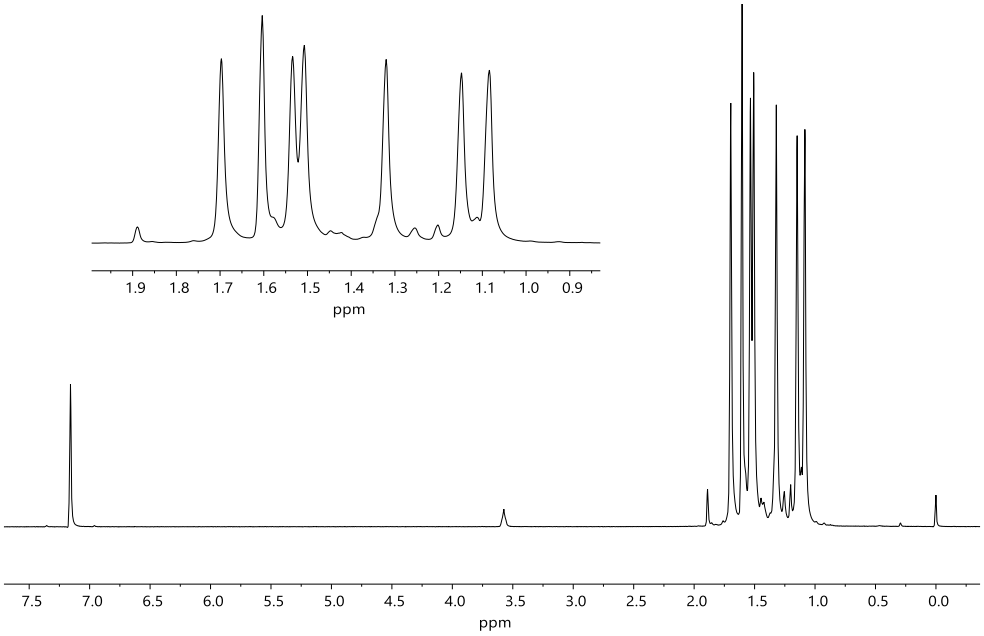

Fig. S21 $^{1}H\{^{31}P\}$ NMR spectrum of **4** in benzene-d^6 (400 MHz).

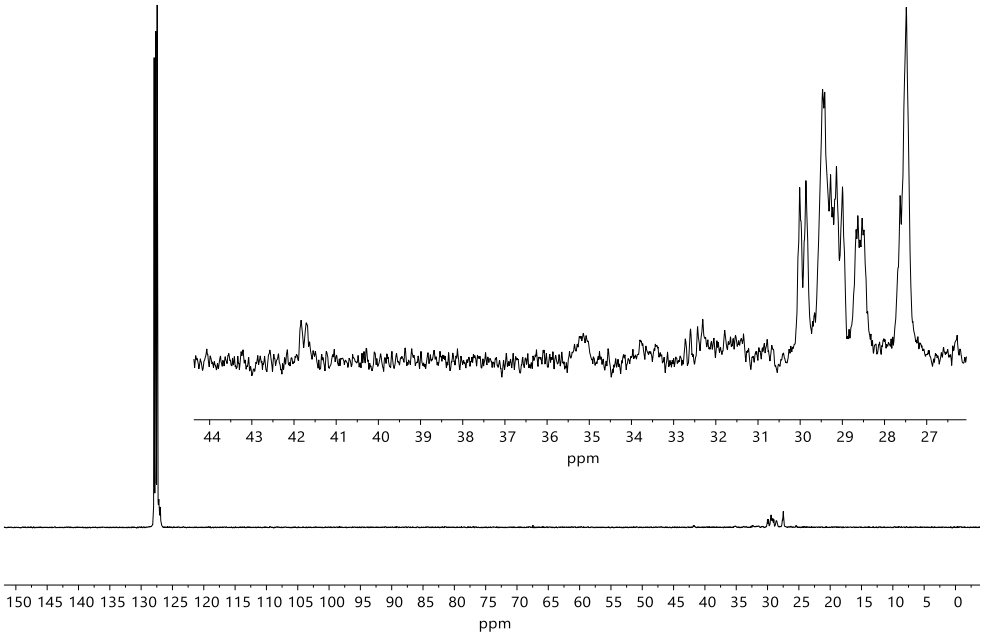

Fig. S22 $^{13}C\{^{1}H\}$ NMR spectrum of **4** in benzene-d^6 (101 MHz).

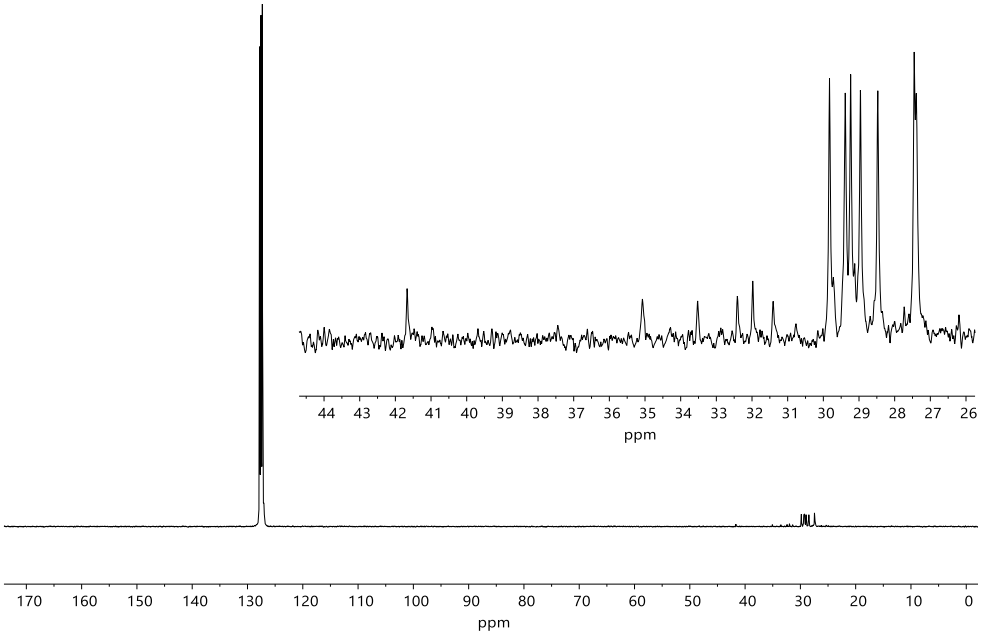

Fig. S23 $^{13}C\{^{1}H,^{31}P\}$ NMR spectrum of **4** in benzene-d^6 (101 MHz).

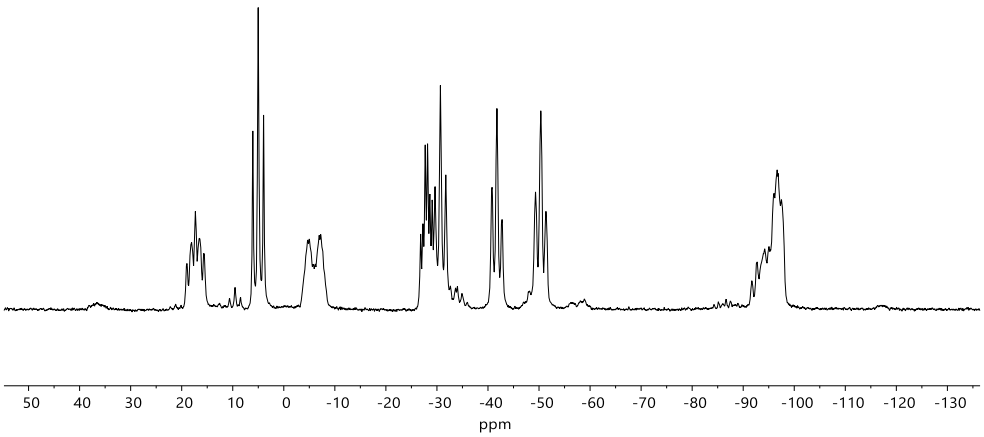

Fig. S24 $^{31}P\{^{1}H\}$ NMR spectrum of **4** in benzene-d^6 (162 MHz).